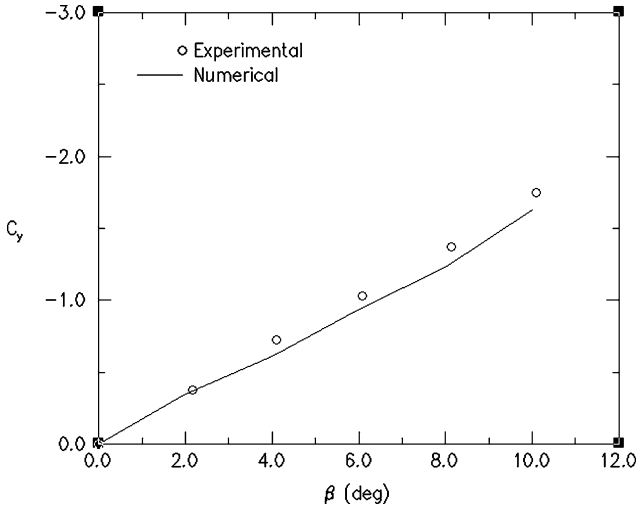

Fig. 4 Titan IV side-force coefficient.

might be an issue in the regions of flow separation as it is impossible to know a priori the origins and trajectories of the multiple vortices trailing off the many components of the vehicle. Similar to the pitch simulations, the yaw simulations generated slight forces in the pitch direction as a result of the asymmetries of the vehicle.

Conclusions

The flow solver, UBIFLOW, was developed with the goal of producing efficient, accurate flow solution software capable of handling complex configurations. In the work presented here, UBIFLOW's ability to simulate the flowfield of complex configurations was tested on a couple of launch vehicles. The predictive capability of UBIFLOW was demonstrated through the use of sample launch configurations for which experimental data were available. Computational results were presented for these high-incidence-angle configurations in the transonic speed regime to evaluate the accuracy and reliability of the UBIFLOW code. Considering the assumptions in the viscous model used in this study, that is, the thin-layer assumption and the simple algebraic turbulence model, the agreement with experimental data is thought to be excellent for the pitch simulations and good for yaw simulations.

Acknowledgments

The authors thank Lockheed Martin Corp. and Victor Whitehead for supporting this effort. In addition, Peter Huseman, our Technical Monitor, is to be credited with steering us in the direction of high incidence angle maneuvers. The authors also thank Joe Bomba of Lockheed Martin for his assistance in acquiring geometry and experimental data and in reducing the raw numerical data for comparison.

References

[1]Arabshahi, A., "A Dynamic Multiblock Approach to Solving the Unsteady Euler Equations About Complex Configurations," Ph.D. Dissertation, Dept. of Aerospace Engineering, Mississippi State Univ., Mississippi State, MS, May 1989.

[2]Thomas, P. D., and Lombard, C. K., "Geometric Conservation Law and Its Application to Flow Computations on Moving Grids," *AIAA Journal*, Vol. 17, No. 10, 1979, pp. 1030–1037.

[3]Tannehill, J. C., Anderson, D. A., and Pletcher, R. H., *Computational Fluid Mechanics and Heat Transfer*, 2nd ed., Taylor and Francis, Washington, DC, 1997.

[4]Ortega, J. M., and Rheinboldt, W. C., *Iterative Solution of Nonlinear Equations in Several Variables*, Academic Press, New York, 1970.

[5]Vanden, K. J., "Direct and Iterative Algorithms for Three-Dimensional Euler Equations," Ph.D. Dissertation, Dept. of Aerospace Engineering, Mississippi State Univ., Mississippi State, MS, Dec. 1992.

[6]Roe, P. L., "Approximate Riemann Solvers, Parameter Vectors, and Difference Schemes," *Journal of Computational Physics*, Vol. 43, No. 2, 1981, pp. 357–372.

[7]Osher, S., and Chakravarthy, S., "Very High Order Accurate TVD Schemes," ICASE Rept. 84-44, Sept. 1984.

[8]van Leer, B., "Toward the Ultimate Conservative Difference Scheme. V. A Second Order Sequel to Godunov's Method," *Journal of Computational Physics*, Vol. 32, No. 1, 1979, pp. 101–136.

[9]Whitfield, D. L., Janus, J. M., and Simpson, L. B., "Implicit Finite Volume High Resolution Wave-Split Scheme for Solving the Unsteady Three-Dimensional Euler and Navier–Stokes Equations on Stationary or Dynamic Grids," Engineering and Industrial Research Station, Mississippi State Univ., Rept. MSSU-EIRS-ASE-88-2, Mississippi State, MS, Feb. 1988.

[10]Gatlin, B., "An Implicit, Upwind Method for Obtaining Symbiotic Solutions to the Thin-Layer Navier–Stokes Equations," Ph.D. Dissertation, Dept. of Mechanical and Nuclear Engineering, Mississippi State Univ., Mississippi State, MS, Aug. 1987.

[11]Baldwin, B. S., and Lomax, H., "Thin-Layer Approximation and Algebraic Model for Separated Turbulent Flows," AIAA Paper 78-257, Jan. 1978.

[12]Degani, D., and Schiff, L. B., "Computation of Turbulent Supersonic Flow Around Pointed Bodies Having Crossflow Separation," *Journal of Computational Physics*, Vol. 66, No. 1, 1986, pp. 173–196.

[13]Arabshahi, A., and Janus, J. M., "A Multiblock Compressible Navier–Stokes Solver Applied to Complex Launch Vehicles," AIAA Paper 99-3378, June–July 1999.

[14]Whitmire, J. B., "A Numerical Simulation of the Lockheed-Martin Titan IV Booster," M.S. Thesis, Dept. of Aerospace Engineering, Mississippi State Univ., Mississippi State, MS, May 1995.

[15]Remotigue, M., and Jiang, M. Y., "GUM-B Grid Generation Code and Applications," *Proceedings of the 6th International Conference*, edited by M. Cross, B. K. Soni, J. F. Thompson, J. Hauser, and P. R. Eiseman, International Society of Grid Generation, NSF Engineering Center for Computational Field Simulation, College of Engineering, Mississippi State Univ., Mississippi State, MS, 1998, pp. 823–832.

R. Cummings
Associate Editor

Parametric Scaling Model for Nongeosynchronous Communications Satellites

Philip N. Springmann* and Olivier L. de Weck†
Massachusetts Institute of Technology, Cambridge, Massachusetts 02139

Nomenclature

g	=	acceleration caused by gravity, m/s^2
I_{sp}	=	specific impulse, s
M_{dry}	=	spacecraft dry mass, kg
M_{PL}	=	payload mass, kg
M_{pp}	=	primary power mass, kg
M_{prop}	=	propellant mass, kg
M_{wet}	=	spacecraft wet mass, kg
M_0	=	premaneuver spacecraft mass, kg
N	=	number of data points
P_{bol}	=	total power at beginning of life, W
P_{eol}	=	total power at end of life, W
P_{PL}	=	payload power, W

Presented as Paper 2003-2310 at the 21st International Communications Satellite Systems Conference, Yokohama, Japan, 15–19 April 2003; received 3 November 2003; revision received 19 February 2004; accepted for publication 25 February 2004.

*Undergraduate Research Assistant, Department of Aeronautics and Astronautics. Student Member AIAA.

†Assistant Professor, Department of Aeronautics and Astronautics, Engineering Systems Division. Member AIAA.

T_{life} = system design lifetime, years
V_{sat} = satellite volume, m^3
ΔV = velocity increment, m/s
σ = rms deviation

Introduction

THE size of the design space for satellite communications systems presents a major difficulty during the conceptual design phase. In considering a future system, it is not feasible to develop all possible design options in detail from the ground up. Most system trade studies[1] rely to some extent on scaling relationships (e.g., mass- or power-estimating relationships) derived from quality empirical data. Available data for communications satellites apply primarily to geosynchronous-orbit (GSO) systems. There is, however, renewed interest in non-GSO systems in low- and mid-Earth orbit (LEO, MEO). Unfortunately, scaling models currently available in the literature are too general or outdated and do not give information about their uncertainty and range of applicability.

This Note therefore develops an updated parametric scaling model, specifically for nongeosynchronous (NGSO) communications satellites. The first step is to collect empirical data on which such a scaling model can be based. The number of operational NGSO systems is small and would not, by itself, represent a statistically sufficient data set. Presently, only Iridium, Globalstar, and Orbcomm are operational, although an intermediate-circular-orbit test satellite was successfully launched in June 2001. The approach of this Note is therefore to use technical descriptions of 36 proposed NGSO systems, which have been extracted from license applications filed with the Federal Communications Commission (FCC) in the February 1990–May 1999 time frame. The second step consists of data analysis and model building. The response surface method (RSM) is used to derive empirical scaling relationships among important system-level parameters. The third step is to benchmark the new scaling model against actual deployed systems and to quantitatively compare it to previous models.

Literature Review

Pritchard[2] originally developed a set of mass and power estimating relationships for communications satellites based on data from the 1970 and 1980 periods. Richharia[3] has reproduced this model in a more recent reference.

Larson and Wertz[4] have compiled an exhaustive set of guidelines for various aspects of space system design. These include mass- and power-estimating relationships as well as procedures for developing propellant, mass, and power budgets. Their identification of spacecraft configuration drivers for mass- and power-estimating relationships formed starting points in the development of our model. Saleh et al.[5] have expanded on the work of Larson and Wertz, focusing on the effects of increasing system design lifetimes on spacecraft mass and cost.

There are a number of drawbacks to the existing scaling models. In some cases, the data underlying the models are out of date as a result of ongoing technical innovation. Moreover, these models are applicable to a very general class of satellites. This can include spacecraft designed not only for communications, but for navigation, remote sensing, or other scientific or military purposes. In addition, little information is available as to the uncertainty in these models or their applicability to various classes of satellites. Our aim is to develop a model focused specifically on NGSO communications spacecraft that will give designers of such systems higher-fidelity estimating relationships. In addition, we would like to provide quantitative measures of uncertainty.

Data Mining

Federal Communications Commission Filings

Between 1990 and 1999 a number of organizations filed with the FCC for licenses to operate NGSO satellite communications systems. These filings are publicly available based on the Freedom of Information Act of 1966, commonly known as the FOIA (5 U.S.C. §552). The filings serve two purposes. First, they are an integral part of the FCC and International Telecommunication Union licensing process and as such must demonstrate the technical feasibility of a particular project. Second, they help the FCC assign specific frequency bands for service, feeder, and intersatellite links. Obtaining FCC approval and acquiring the right to use desired frequency bands has become a major hurdle that new and existing communications satellite operators need to clear. A substantial amount of effort goes into the development of a license application.

Each filing contains a technical description of the space, ground, and user segments of the proposed system. Because the viability of the proposed system must be established, numerical values for important system-level parameters are provided. This has allowed us to systematically extract numerical data on communications system and network design, constellation architecture, spacecraft bus design, system cost, and setup of gateways and user terminals for 36 proposed NGSO satellite communications systems. The resulting data set, which forms the basis of the subsequent analysis, is contained in Table 1. What follows is a brief summary of this data and a look at some apparent trends in NGSO communications satellite design.

LEO Communications Systems

The Federal Aviation Administration's Associate Administrator for Commercial Space Transport divides the LEO satellite communications market into three segments (Fig. 1) termed little LEO, big LEO, and broadband LEO. The term LEO is used loosely here; approximately one-third of the systems surveyed actually employ medium-Earth-orbit (MEO) constellations above 2000-km altitude.

Little LEO systems like Orbcomm operate at frequencies below 1 GHz using less than 1 MHz of bandwidth. Their capabilities are limited to paging, data acquisition, asset monitoring, and the like. Often these systems neither require nor provide continuous global coverage. Big LEO systems are more or less analogous to terrestrial cellular networks, offering personal voice and in some cases low-rate data communications services. Iridium and Globalstar both fall into this segment. Big LEO systems generally operate at frequencies between 1 and 7 GHz and utilize 10–100 MHz of bandwidth. Finally, broadband LEO systems offer high-speed data and multimedia services operating in the Ku, Ka, Q, and V bands, utilizing up to 3 GHz of bandwidth.

On the whole, proposed communications spacecraft have become larger and more powerful in the past 10 years, in step with the trend toward broadband systems. The highest launch masses belong to large broadband systems; however, other factors such as payload power and onboard propellant contribute more directly to launch mass than increasing bandwidth requirements. Other factors contributing to the increasing size and power of communications spacecraft include more ambitious service requirements as well as increasing orbital altitudes and design lifetimes. Although system

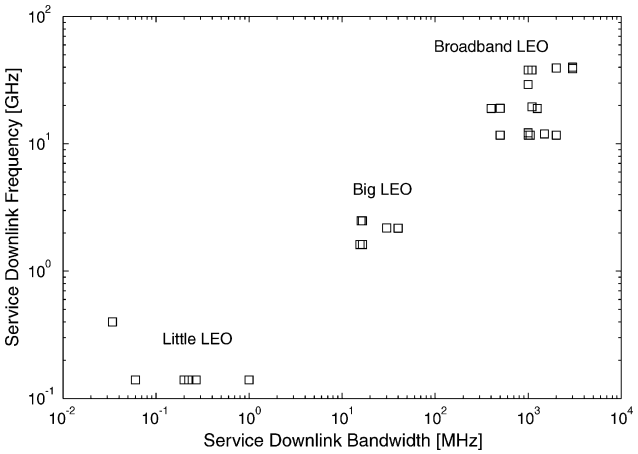

Fig. 1 Service downlink center frequency plotted against service downlink bandwidth requirement.

Table 1 NGSO communications satellite systems: data set extracted from FCC filings from February 1990 to May 1999

System	Filing date	No. sats	T_{life}, years	Alt., km	Downlink BW, MHz[a]	Downlink CFreq, GHz[b]	M_{dry}, kg	M_{prop}, kg	M_{wet}, kg	M_{pl}, kg	P_{PL}, W	P_{bol}, W	P_{eol}, W
@contact	May 99	20	12	10,400	1,100	19.55	2,542	870	3,412	583	6,264	——	——
AMSC NGSO	Nov. 94	10	10	10,355	16.5	2.49	2,450	600	3,050	950	4,500	——	4,900
Boeing NGSO	Jan. 99	20	12	20,182	1,000	12.20	2,118	1,743	3,861	1,217	9,500	14,201	10,678
Celestri	June 97	63	8	1,400	1,000	29.30	2,500	600	3,100	——	——	13,600	4,600
Constellation	June 91	48	5	1,018.6	16.5	2.49	113.4	11.3	124.7	34.5	49	250	49
Ellipso	Nov. 90	24	5	875	16	2.49	68	0	68	——	——	360	120
E-Sat	Nov. 94	6	10	1,261	1	0.14	100	14	114	——	——	——	200
Final Analysis	Nov. 94	24	7	1,000	0.225	0.14	98.5	0	98.5	——	29.5	59	47
GE LEO	Nov. 94	24	5	800	0.034	0.40	15	0	15	——	11	10.56	9.1
GEMnet	Nov. 94	38	5	1,000	1	0.14	——	——	45	——	——	——	——
Globalstar	June 91	48	7.5	1,389	16.6	1.62	222	40	262	60	50	875	150
Globalstar 2GHz	Sept. 97	64	7.5	1,420	40	2.18	676	156	832	300	1,200	3,000	1,520
Globalstar GS40	Sept. 97	80	7.5	1,440	1,000	38.00	992	234	1,226	——	——	4,500	2,280
HughesLINK	Jan. 99	22	12	15,000	1,000	11.73	2,540	400	2,940	1,000	6,000	10,500	9,100
HughesNET	Jan. 99	70	10	1,490	500	11.73	1,650	350	2,050	600	4,000	8,200	7,500
ICO	Sept. 97	10	12	10,355	30	2.19	2,413.8	336.2	2,750	898	5,994	——	9,000
Iridium	Dec. 90	77	5	765	15.5	1.62	299.4	41.3	340.7	165.1	686	——	1,429
Iridium Mcell	Sept. 97	96	7.5	853	40	2.18	1,442	271	1,713	670	1,105	7,300	——
Leo One	Sept. 94	48	5	950	0.2	0.14	154	0	154	26	158	——	290
LM MEO	Dec. 97	32	10	10,352	3,000	40.00	2,133	38	2,171	840	6,610	——	8,760
M Star	Sept. 96	72	8	1,350	3,000	39.00	2,210	323	2,535	——	——	3,100	1,530
Odyssey	May 91	12	10	10,371	16.5	2.49	1,620	880	2,500	450	1,200	——	1,800
Orbcomm	Feb. 90	20	7	970	0.27	0.14	145	5	150	——	325	450	360
Orblink	Sept. 97	7	7	9,000	1,000	38.00	1,268	742	2,010	615	3,650	——	4,010
Pentriad	Sept. 97	13	——	HEO	2,000	39.50	1,455	684	2,139	592	100	10,247	7,684
SkyBridge	Feb. 97	64	8	1,457	1,050	11.73	——	——	800	300	2,150	——	3,000
SkyBridge II	Dec. 97	96	10	1,468	1,250	19.00	——	——	2,650	1,000	5,000	——	9,000
Spaceway	Dec. 97	20	12	10,352	500	19.05	2,500	350	2,850	——	7,500	13,800	10,000
StarLynx	Sept. 97	20	12	10,352	1,100	38.05	3,050	450	3,500	——	——	17,000	15,000
StarSys	May 90	24	5	1,300	1	0.14	112	0	112	24	84	——	125
Teledesic	Mar. 94	840	10	700	400	19.00	747	48	795	173	3,600	11,595	6,626
Teledesic Ku	Jan. 99	30	7	10,320	2,000	11.70	1,132	192	1,324	——	1,200	6,500	1,500
Teledesic V	Sept. 97	72	7	1,375	1,000	38.00	566	48	614	——	600	5,000	800
TRW EHF	Sept. 97	15	15	10,355	3,000	39.00	2,707	3,227	5,934	926	15,000	——	15,500
Virgo	Jan. 99	15	12	20,281	1,500	11.95	2,778	252	3,030	1,058	9,900	——	10,593
VITA	Sept. 90	2	5	805.5	0.06	0.14	43	2.5	45.5	——	——	42	25.3

[a]BW = bandwidth. [b]CFreq = center frequency.

design lifetimes have not increased uniformly over the past decade, design lifetimes of 10 years or more have become more common since 1997. The same is true for orbital altitudes: MEO designs are much more prevalent after 1997.

Limitations

Although we consider these data a suitable basis for an empirical model, the use of data from systems at the proposal stage has some limitations. First, it is to be expected that some of the parameter estimates in the FCC filings are overly optimistic. The degree to which these estimates are realistic varies. Some of the filings do include margins in their mass and power budgets, whereas others do not. In any case, it is difficult to systematically correct for overly hopeful estimates. This is one source of uncertainty in the models. This issue can be partially addressed by benchmarking scaling models against fielded systems.

Empirical Model Building

For our purposes, RSM is a set of techniques that uses adequate measurements of the response of interest and determinines a mathematical model that best fits the data collected. RSM is similar to regression analysis in that relationships between explanatory and response variables are established empirically.

What follows is a brief review of the mathematics underlying empirical modeling.[6] Consider the model

$$y = f(\boldsymbol{x}, \theta) + \varepsilon \tag{1}$$

where $\boldsymbol{x} = [x_1, x_2, \ldots, x_k]^T$ are independent, explanatory variables; $\theta = [\theta_1, \theta_2, \ldots, \theta_k]^T$ are unknown parameters; and ε is an (unknown) error term. The least-squares estimate of θ is obtained by minimizing the function

$$S(\theta) = \sum [f(\boldsymbol{x}, \theta) - \hat{\boldsymbol{y}}_u]^2 \tag{2}$$

where $\hat{y}_u$ is the uth observed value of the response at the point $x_{u1}, x_{u2}, \ldots, x_{uk}$; $u = 1, 2, \ldots, N$. The rms deviation, one measure of model uncertainty, is the square root of the sum of residual squares divided by the number of observations:

$$\sigma = \sqrt{S(\hat{\theta})/N} \tag{3}$$

Mass

We begin our analysis by considering spacecraft mass. Designers rely a great deal on mass-estimating relationships because obtaining a bottom-up estimate for the mass of a spacecraft requires detailed knowledge about its design. In general, the dry mass of a satellite is influenced primarily by the mass of its payload, which in turn is driven by the payload power. On a communications satellite, the bulk of the payload power requirement owes to the power of the transmitters, transponders, and receivers comprising the payload.[3]

The relationship between dry mass M_{dry} and payload power P_{PL}, based on the data in Table 1, is best described by a power law model of the form:

$$M_{dry} = 7.5 P_{PL}^{0.65} \tag{4}$$

This (as well as each of the other scaling relations) is valid as long as the quantities are used in the units shown in the nomenclature.

The data show a slightly better correlation between wet mass and payload power than dry mass and payload power; the relationship for wet mass is

$$M_{wet} = 4.6 P_{PL}^{0.73} + 140 \tag{5}$$

This relationship is shown as the solid line in Fig. 2.

Table 2 Comparison of wet mass models before and after inclusion of propellant mass

Equation	Variables	σ, kg	95% CI, kg[a]
(5)	P_{PL}	551	±382
(6)	P_{PL}, M_{prop}	301	±199

[a]CI = average confidence interval.

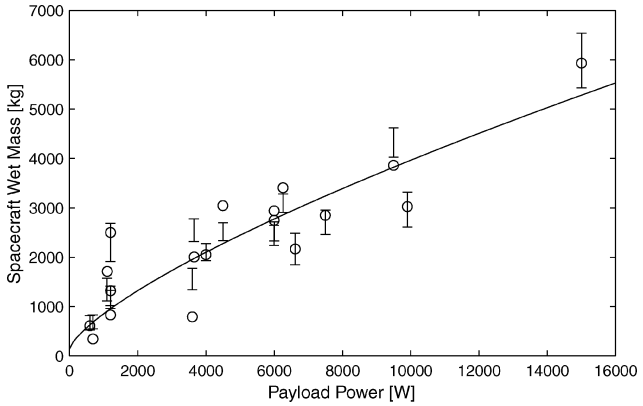

Fig. 2 Wet mass estimates using Eq. (6) with 95% confidence intervals superimposed over the FCC data; ——, follows Eq. (5).

The estimates from Eq. (5) can be improved if another explanatory variable, propellant mass, is introduced into the model:

$$M_{wet} = 38(0.14P_{PL} + M_{prop})^{0.51} \tag{6}$$

Propellant can account for anywhere from a very small portion to as high as 35–45% of a spacecraft's wet mass, depending more fundamentally on the design altitude, design lifetime, and stabilization scheme of the system. Estimates computed using this improved relationship are shown with their corresponding data points and 95% confidence intervals in Fig. 2. This is the first published attempt at modeling wet mass as a function of two variables, and it represents an improvement over modeling wet mass as a function of payload power alone. The two wet mass models from Eqs. (5) and (6) are compared in Table 2.

Wet mass is estimated using a power law rather than a linear relationship as has traditionally been done.[2,3] One might hypothesize that the shallowing nature (i.e., an exponent smaller than 1) of the mass-estimating relationships is caused by economies of scale for large systems.

Propellant Mass

If propellant mass is to be used to improve a wet mass estimate, the designer must be able to estimate accurately the propellant mass requirement from more fundamental design variables. We were able to duplicate over half of the propellant mass estimates in the FCC filings to within 25% using an initial wet mass estimate, design altitude, design lifetime, and method of attitude control, despite making several simplifying assumptions.

The first step toward estimating propellant mass is establishing a ΔV budget. This budget includes allowances for orbit injection, drag compensation, attitude control, and deorbit at end of life. Once the ΔV budget is established, the required propellant mass is given by

$$M_{prop} = M_0\left[1 - e^{-(\Delta V/I_{sp}g)}\right] \tag{7}$$

In Eq. (7), M_0 is the spacecraft mass before a maneuver is completed. For example, it is the launch mass of the system if the propellant mass for orbit injection is being calculated.

In our calculations, a solid-rocket apogee kick motor ($I_{sp} = 290$ s) was assumed for orbit injection, and monopropellant hydrazine ($I_{sp} = 210$ s) was assumed for all maneuvers following orbit injection. In addition, we assumed a transfer orbit with a perigee at an altitude of 150 km and an apogee at the design altitude. In computing the required ΔV, it was assumed that the apogee kick motor would circularize the transfer orbit at the design altitude. Somewhat arbitrary but reasonable parameters were used to compute ΔV for drag compensation and attitude control: these are summarized in Tables 3 and 4. In future work, antenna size and solar panel size might be used along with altitude to estimate the required ΔV for drag compensation. Finally, it was assumed that deorbit would be accomplished by changing the cirular orbit to an elliptical one with a perigee at the surface of the Earth.

Table 3 M_{prop} estimation parameters: drag compensation

Altitude, km	ΔV, m/s per year
<500	12
500–600	5
600–1000	2
>1000	0

Table 4 M_{prop} estimation parameters: attitude control

Type	ΔV
Gravity gradient	0
Three-axis	10
Margin	22%

Table 5 Typical subsystem masses as percentages of spacecraft dry mass (adapted from Ref. 5)

Subsystem	% M_{dry} (std. dev.)
Payload	27 (4)
Attitude control	7 (2)
Electrical power	32 (5)
Propulsion	4 (1)
Structure	21 (3)
Thermal	4 (2)
Tracking and command	5 (2)
Total	100

Fuel type or method of orbit injection or deorbit are examples of parameters that could be changed without making the computation substantially more difficult. Thus, it is reasonable to expect to be able to estimate the propellant mass requirement accurately. Beginning with an initial wet mass estimate made using Eq. (5), an estimate of the propellant mass requirement can be obtained (Tables 3 and 4) and the wet mass estimate in turn refined using Eq. (6).

Intersatellite Links

It was hypothesized that the effect of intersatellite links (ISL) on spacecraft mass was significant and could be deduced from the FCC data. However, no statistically significant effect was found. This is most likely caused by a variation in ISL implementations, that is, the number of intersatellite links on each spacecraft and the type of link employed (e.g., RF, optical) varied among the systems surveyed.

Subsystem Masses

If both wet mass and propellant mass are known, the dry mass of a satellite is given by

$$M_{dry} = M_{wet} - M_{prop} \tag{8}$$

Payload and other subsystem masses are best estimated as percentages of the spacecraft dry mass. Data from the FCC filings are too sparse to provide a reasonable basis for estimating the mass percentages of subsystems other than payload. The percentages compiled by Saleh et al.[5] appear to be most helpful. These are summarized in Table 5. Our analysis found the average dry mass percentage of the payload to be 36% with a standard deviation of 11%, both somewhat higher than the values in Table 5.

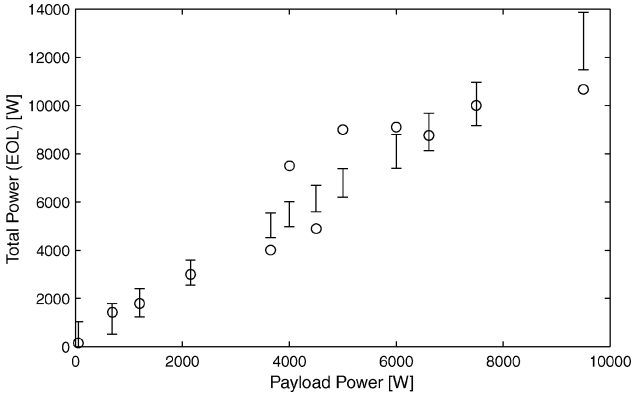

Fig. 3 P_{eol} estimates using Eq. (9) with 95% confidence intervals.

Power

The total power requirement drives the size and mass of the solar arrays. Starting with a value for spacecraft power at end of life, the beginning-of-life requirement can be computed along with the surface area and mass of the solar array. Total spacecraft power at end of life appears to scale linearly with payload power:

$$P_{\text{eol}} = 1.3P_{\text{PL}} + 261 \tag{9}$$

This relationship is shown in Fig. 3. The rms deviation is 970 W. The total power requirement at end-of-life is related to the beginning-of-life requirement by

$$P_{\text{eol}} = P_{\text{bol}} \times L_d \tag{10}$$

Life degradation L_d is a function of the system design lifetime as well as the degradation per year. The degradation per year, in turn, depends on a number of other factors, including orbital parameters and properties of the solar array. A more complete discussion of life degradation can be found in Larson and Wertz.[4]

Volume and Specific Power

The relationship between spacecraft (folded) volume, mass, and power is critical for estimating launch needs. The subsequent numbers are based on a smaller subset of the FCC data ($N \approx 12 - 16$). In the early stages of design, the volume of a spacecraft is typically estimated by dividing its launch (wet) mass by an appropriate density value.[4] The slope of a linear regression line of folded volume V_{sat} vs M_{wet} suggests an average density of 285 kg/m^3, significantly higher than the typical range of 20–172 given by Larson and Wertz.[4] One hypothesis is that miniaturization of components, electronics, and tighter systems integration has led to higher spacecraft densities relative to systems in the 1970s and 1980s. The average dry mass density of the surveyed FCC satellites was 194.7 kg/m^3. However, the relatively large scatter in the data ($\sigma = 186.1$ kg/m^3) makes it difficult to derive a definite scaling law for spacecraft volume. Folded spacecraft volumes varied widely between 0.65–17.3 m^3 with an average of 5.99 m^3. In some cases (e.g., Iridium) the maximum number of satellites per launch vehicle is limited by risk considerations rather than by payload fairing volume or launcher lifting capacity.

Specific power for NGSO satellites ranged from 0.93 W/kg for small satellites ($P_{\text{bol}} = 150$ W) to 11.85 W/kg for large systems ($P_{\text{bol}} = 10678$ W), supporting the earlier statement that generally some economies of scale are achieved for larger platforms. Average specific power $P_{\text{bol}}/M_{\text{dry}}$ was 6.00 W/kg, but as in the case of spacecraft volume there is significant scatter in specific power estimates with a standard deviation of 3.58 W/kg.

Applicability

The models developed in this paper appear to be most useful in the design of larger NGSO spacecraft, namely, where $P_{\text{PL}} \in [1, 16]$ kW, as the confidence intervals will be a smaller percentage of the estimates for larger systems. However, in the cases of the mass- and power-estimating relationships there were no serious outliers (i.e., $|y_u - \hat{y}_u| > 2\sigma$). This suggests that the models are still of at least limited use over all sizes of NGSO communications satellites.

Table 6 Benchmarking of wet mass model in Eq. (6) using existing systems

System	P_{PL} Act.,[a] W	M_{prop} Act., kg	M_{wet} Est.,[b] kg	M_{wet} Act., kg	Model error, %
Globalstar	1000	50	552.0	450	22.7
Iridium	1400	115	725.8	689	3.0

[a]Act. = actual. [b]Est. = estimate.

Table 7 Comparison of wet mass model with earlier models based on data in Table 1

Equation no., model	Avg. error, %	RMS error, kg
(11), (12) Pritchard/Richharia	−4.4	727
(13) Larson/Wertz	14.4	955
(6) de Weck/Springmann	1.6	301

Comparison with Earlier Models

We now proceed to compare the wet mass model developed in the preceding section with earlier models. First, we consider the model presented by Pritchard[2] and Richharia.[3] Richharia[3] estimates wet mass in the following manner. First, dry mass is estimated as a function of the payload mass M_{PL} and the primary power mass M_{pp}:

$$M_{\text{dry}} = 2.0(M_{\text{PL}} + M_{\text{pp}} - 10) \tag{11}$$

This relationship is valid for three-axis stabilized spacecraft. The primary power mass includes solar arrays, batteries, and power control hardware. Our data yielded a rough estimate of the primary power mass as approximately 24% of the dry mass. We substitute this for M_{pp} into Eq. (11) in our calculations. Wet mass is then estimated using

$$M_{\text{wet}} = M_{\text{dry}} e^{(100+5T_{\text{life}})/gI_{\text{sp}}} \tag{12}$$

A nominal I_{sp} of 260 s was used in our calculations.

The model presented by Wertz and Larson[4] estimates that the payload mass is 30% of the dry mass, on average. That implies that M_{dry} (total) $= 3.3 \times M_{\text{PL}}$. Propellant mass is estimated at between 0–25% of the dry mass. We take the high end of the latter estimate (25%) and from Eq. (8) arrive at

$$M_{\text{wet}} \approx 4M_{\text{PL}} \tag{13}$$

The proposed scaling model in Eq. (6) is benchmarked in Table 6 using the existing Iridium and Globalstar systems.[7] In both cases, the model overestimated the wet mass of the system, although only slightly for Iridium. Equations (6) and (11–13) are compared in Table 7 using the data in Table 1. On the basis of both average percent error and rms deviation, our model represents an improvement over the earlier two. This is to be expected, as the comparison is made using the NGSO data underlying our model. The intent here is to show the need to continually update and improve scaling models, while providing insight into their range of applicability.

Conclusions

A parametric model for nongeosynchronous orbit communications spacecraft was developed in this Note using data obtained from FCC filings. Trade studies during conceptual design depend fundamentally on such scaling models. Intermediate parameters like mass, power, and volume directly influence performance and cost. The presented scaling model can predict wet mass for nongeosynchronous communications satellites with an average error of 1.6%, which represents an improvement over previous models. There is some limitation to the accuracy of the scaling law as a result of the conceptual nature of the underlying FCC data. We note that the actual wet mass of an Iridium satellite is 689 kg, including 115 kg of propellant, both more than twice the figure in Iridium's original FCC filing. Using our equation, the wet mass estimate at the filing date would have been 467 kg (vs the 340.7 kg given in the FCC filing). The estimate for the deployed spacecraft is 725.8 kg. Although estimates will fluctuate as a result of scope and design

changes between the proposal stage and actual deployment, the inclusion of propellant mass in the equation derived for spacecraft wet mass allows changes to the design lifetime and design altitude to be explicitly taken into account.

Acknowledgments

This work was supported in part by the Meryl and Stewart Robertson UROP Fund in conjunction with the Massachusetts Institute of Technology Undergraduate Research Opportunities Program. This research was also funded by the Alfred P. Sloan Foundation under Grant 2000-10-20 for the development of Engineering Systems Studies with Gail Pesyna serving as the Program Monitor.

References

[1]de Weck, O. L., and Chang, D. D., "Architecture Trade Methodology for LEO Personal Communication Systems," AIAA Paper 2002-1866, May 2002.

[2]Pritchard, W. L., "Estimating the Mass and Power of Communications Satellites," *International Journal of Satellite Communications*, Vol. 2, No. 2, 1984, pp. 107–112.

[3]Richharia, M. *Satellite Communications Systems: Design Principles*, McGraw–Hill, New York, 1995, pp. 300–306.

[4]Larson, W. J., and Wertz, J. R. (eds.), *Space Mission Analysis and Design*, 3rd ed., Microcosm Press, El Segundo, CA, and Kluwer Academic, Boston, 2001, Chap. 10.

[5]Saleh, J. H., Hastings, D. E., and Newman, D. J., "Spacecraft Design Lifetime," *Journal of Spacecraft and Rockets*, Vol. 39, No. 2, 2002, pp. 244–257.

[6]Khuri, A. I., and Cornell, J. A., *Response Surfaces: Designs and Analyses*, Marcel Dekker, New York, 1996.

[7]Lutz, E., Werner, M., and Jahn, A., *Satellite Systems for Personal and Broadband Communications*, Springer-Verlag, New York, 2000, pp. 375–378, 389–395.

J. Korte
Associate Editor

Analysis of Optimal Weaving Frequency of Maneuvering Targets

Rafael Yanushevsky*
Technology Service Corporation, Silver Spring, Maryland 20910

Nomenclature

a_c = guidance command, m^2/s
a_L = missile acceleration, m^2/s
a_T = target acceleration, m^2/s
N = effective navigation ratio
t_{go} = time to go, s
V_{cl} = closing velocity, m/s
y = relative separation between a missile and target, m
ζ = flight-control system damping
λ = line-of-sight angle, rad
τ = flight-control system time constant, s
ω = flight-control system natural frequency, rad/s
ω_z = airframe zero frequency, rad/s

Introduction

MANEUVERS present the best strategy for missiles to achieve their goals. Sinusoidal or weave maneuvers of a target can make it difficult for a pursuing missile to obtain an intercept. Optimal control and game theory have been used in attempts to formulate precisely and solve the problems of optimal pursuit and evasion.[1–4] Unfortunately, it is difficult to build a realistic analytical model that can be utilized in practice. Deterministic optimal control laws require full information about a target and missile flight parameters. Such complete information is never available. However, it is reasonable to assume that the evader (target) knows the types of missiles and guidance laws that can be used for interception, but does not know the time to go until intercept of the pursuing missile. In this case, a properly chosen periodic maneuver sequence offers the target its best chance of survival.[5,6]

Miss distances depend on the frequency of maneuvers. It is shown that their functional relationship has a maximum, that is, there exists a frequency for which the amplitude of the miss distance has a maximum. The procedure of determination of the optimal frequency is presented.

This Note considers the influence of the target weave maneuver on a third-order proportional navigation guidance system, presented in the form that is commonly used in practice. The analogous analysis for a simplified first-order proportional navigation guidance system is given in Ref. 6. The generalized analysis in this Note makes it possible to utilize in practice the relations obtained. A closed-form solution for the miss distance as a function of the effective navigation ratio, guidance system time constant, natural frequency, and damping and weave maneuver amplitude and frequency is derived. The procedure of determination of the optimal frequency, that is, the frequency that maximizes the steady-state miss distance amplitude, is described.

Weave Maneuver Analysis

A block diagram of the guidance system under consideration is given in Fig. 1. It has the same structure as that in Refs. 4–6. Here, missile acceleration n_L is subtracted from target acceleration n_T, and the result is integrated to obtain relative position y, which, at the end of flight t_f, is the miss distance $y(t_f)$. A division by range (closing velocity V_{cl} multiplied by time to go t_{go} until intercept) yields the geometric line-of-sight (LOS) angle λ, where the time to go is defined as $t_{go} = t_f - t$. It is assumed that the missile seeker, represented as a perfect differentiator, effectively provides a measurement of the rotation rate of LOS from the interceptor to the target. The filter dynamics are neglected. (For the problem under consideration, the time lag of a filter can be taken into account by an increase in the time constant of the flight-control system.) Perfect estimation of the LOS rate is assumed to generate a guidance command n_c based on the proportional navigation law.

The flight-control system guides the missile to follow this acceleration command. The flight-control system dynamics, which combines its airframe and autopilot dynamics, are represented by

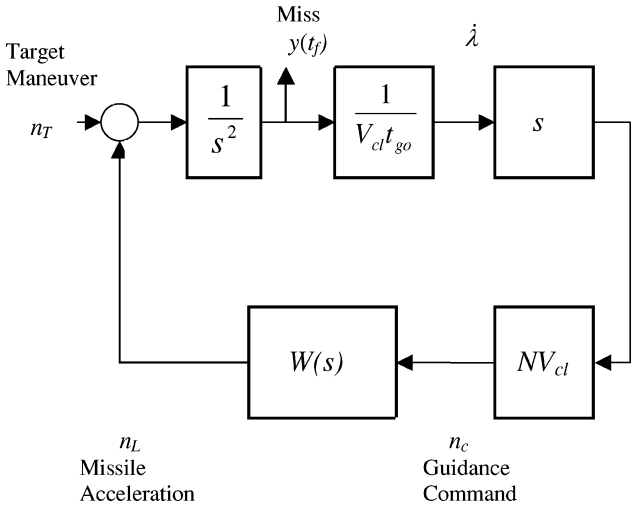

Fig. 1 Missile guidance model.

Received 13 November 2003; revision received 3 March 2004; accepted for publication 3 March 2004.

*Senior Staff Scientist, Missile and Threat Systems Engineering Department, 962 Wayne Avenue, Suite 800.